Letter

# PSR J0952 − 0607 and GW170817: Direct multimessenger constraints on neutron star equation of state through a novel wide-ranging correlation

L. Guo (郭兰) and Y. F. Niu (牛一斐)*

*School of Nuclear Science and Technology, Lanzhou University, Lanzhou 730000, China*
*and Frontier Science Center for Rare Isotopes, Lanzhou University, Lanzhou 730000, China*

(Received 16 November 2023; accepted 28 June 2024; published 22 July 2024)

Our knowledge about neutron star (NS) masses is renewed once again due to the recognition of the heaviest NS PSR J0952 − 0607. By taking advantage of both mass observations of supermassive neutron stars and the tidal deformability derived from event GW170817, a joint constraint on tidal deformability is obtained. A wide-ranging correlation between NS pressure and tidal deformability within the density range from saturation density $\rho_0$ to $5.6\rho_0$ is discovered, which directly yields a constrained NS equation of state (EoS). The newly constrained EoS has a small uncertainty and a softer behavior at high densities without the inclusion of extra degrees of freedom, which shows its potential to be used as an indicator for the component of the NS core.

DOI: 10.1103/PhysRevC.110.L012801

The equation of state (EoS) of nuclear matter is essentially important for both nuclear physics [1] and astrophysics [2]. However, the nuclear EoS is still poorly determined, in particular at high densities or with large isospin asymmetry. Our knowledge about the nuclear EoS mainly comes from the properties of heavy nuclei, where their density is typically limited below the nuclear saturation density $\rho_0 = 2.8 \times 10^{14}$ g cm$^{-3}$ with a relatively small isospin asymmetry $\delta$. Fortunately, neutrons stars (NSs) are one of the most compact forms of matter in the universe with central densities reaching up to 5 to 10 times the nuclear saturation density $\rho_0$ and with very large isospin asymmetry $\delta$ which is nearly 1; i.e., neutrons dominate the nucleonic component of NSs [3], which provide natural laboratories for studying nuclear matter under extreme conditions.

Macroscopic properties of NSs, such as masses, tidal deformabilities, and radii are totally governed by the EoS of NSs [4–6], and thus a great deal of information about the EoS of NSs can be revealed by observations on these properties. Among them, masses are the most widely observed and thus the most informative property, especially those of supermassive NSs [7–13], which can efficiently constrain the NS mass limit $M_{\max}$. The recently discovered supermassive NS PSR J0952 − 0607 [7], with a mass of $M = 2.35 \pm 0.17\ M_\odot$, is the heaviest NS ever known [14]. Combining this discovery with observations of previous supermassive NSs, a new probability distribution function (PDF) of NS mass limit $M_{\max}$, which greatly challenges the stiffness of the neutron star EoSs, is proposed [14]. The discovery of the binary NS merger gravitational-wave (GW) event GW170817 [15] also opened a new window to probe the tidal deformabilities of NSs which are one of the main observables provided by GW signals [16]. It gives a constrained value of a 1.4-solar-mass NS to be $\Lambda_{1.4} = 190^{+390}_{-120}(90\%)$. With the ongoing operation of available GW detectors and the development of the next generation of detectors, tidal deformabilities are going to be determined more accurately in the future.

To utilize such observation information to constrain the NS EoS, the EoS is usually parametrized by different kinds of parametrizations, such as the Taylor-expansion parametrization [17,18], the spectral parametrization [16,19–21], and the piecewise polytropic parametrization [22–26], or constructed by different energy density functionals [27–31]. The corresponding parameters are constrained either directly or through the Bayesian analysis by the observation information. Due to the lack of physics information or good correlations [30,32] between NS observables and EoS parameters, the uncertainties of the constrained EoS are consequently large. Furthermore, limited by the computing resources, the unavoidable cutoff makes the completeness of parameter space usually not as good as what is expected. Therefore, it calls for innovative approaches to constrain the NS EoS in a more direct way.

To achieve such a goal, the key is to explore the direct correlations between macroscopic properties of NSs and microscopic local behaviors. Such studies are rare but with one exception, where the correlation between NS pressure at twice saturation density $p(2\rho_0)$ and the tidal deformability of a 1.4-solar-mass NS, $\Lambda_{1.4}$, was discovered [27,30,33]. If this correlation were universal for a wide density range, the bridge between NS observations and the EoS would be built directly. Therefore, we will explore the universality of this correlation and investigate the possibility to constrain the NS EoS through such a bridge.

In order to adopt more observation information into the above constraint, one also needs to build correlations between different NS observables and tidal deformability. Our knowledge of masses of supermassive NSs are relatively

*Contact author: niuyf@lzu.edu.cn

 

abundant, and recently the supermassive NS PSR J0952 − 0607 updated our knowledge of the NS mass limit again. The correlation between the NS mass limit $M_{\max}$ and the tidal deformability $\Lambda$, although still insufficiently studied [34,35], allows us to convert the abundant mass information into tidal deformability, which can be further used to constrain the EoS. In this work, we propose a novel approach to constrain the NS EoS directly through a wide-ranging correlation between the pressure of the NS and tidal deformability, which at the same time considers the updated information of NS masses. Furthermore, the confidence level of the yielded EoS is obtained through the PDF of each involved quantity, which overcomes the shortage of uncertainty analysis in the previous correlation studies.

In this work, we use 16 EoSs of NSs assuming a crust governed by the Baym-Pethick-Sutherland + Baym-Bethe-Pethick (BPS+BBP) model [36,37] and a pure $npe\mu$ NS core from 16 nucleonic effective interactions, including 9 nonrelativistic ones, MSL0 [38], SGI [39], SIV, SV [40], SKa [41], SkM [42], SLy0 [43], KDE0 [44], and SAMi [45], as well as 7 relativistic ones, DD-ME2 [46], TW99 [47], PKA1 [48], PKDD [49], PKO1 [50], PKO2, and PKO3 [51]. These interactions are chosen under no specific considerations except to ensure their variety; hence, the yielded results can be considered as general as possible. With the obtained EoS, the Tolman-Oppenheimer-Volkoff equations [4,5] and NS tidal deformabilities [6] can be solved and yield the data set $\{p^i(\rho); M^i_{\max}; \Lambda^i_{1.4}\}$, with $p^i(\rho)$ being the $i$th EoS, and $M^i_{\max}$ and $\Lambda^i_{1.4}$ being the NS mass limit and the tidal deformability of a 1.4-solar-mass NS corresponding to the $i$th EoS. We have verified that all quantities involved in this work are not influenced by the choice of the crust EoS, and all results in this work are stable under a moderate change of the members or the size of the interaction pool.

As shown in the main panel of Fig. 1, for the data set $\{M^i_{\max}, \Lambda^i_{1.4}\}$, a good power-law correlation between $M_{\max}$ and $\Lambda_{1.4}$ is discovered since $\{M^i_{\max}, \Lambda^i_{1.4}\}$ can be efficiently fitted using the power function $y = ax^b$ with a coefficient of determination (CoD) of up to $R^2 = 0.91$, which is

$$\Lambda_{1.4} = 11.5346 M^{4.84693}_{\max}. \quad (1)$$

This fitting only gives the most probable $\Lambda_{1.4}$ values for different $M_{\max}$. However, in order to obtain the PDF of $\Lambda_{1.4}$ at each given $M_{\max}$, i.e., $P(\Lambda_{1.4}|M_{\max})$, one can use Eqs. (A1) and (A2) in Appendix A and the corresponding results are shown in shades of red with the color bar in Fig. 1(a).

Considering the fact that the observations of masses of supermassive NSs are relatively abundant compared to the poorly known tidal deformability, the discovered correlation with $R^2 > 0.9$ makes it reliable to use $P(\Lambda_{1.4}|M_{\max})$ as a converter from the information of $M_{\max}$ to that of $\Lambda_{1.4}$. From electromagnetic (EM) observations of supermassive NSs, especially the novel heaviest NS PSR J0952 − 0607, the state-of-the-art distribution about the NS mass limit $P(M_{\max}|\mathrm{EM})$ is extracted in Ref. [14], which is shown in Fig. 1(b). Combining this result with $P(\Lambda_{1.4}|M_{\max})$, the following integration,

$$P(\Lambda_{1.4}|\mathrm{EM}) = \int \mathrm{d}M_{\max} P(\Lambda_{1.4}|M_{\max}) P(M_{\max}|\mathrm{EM}), \quad (2)$$

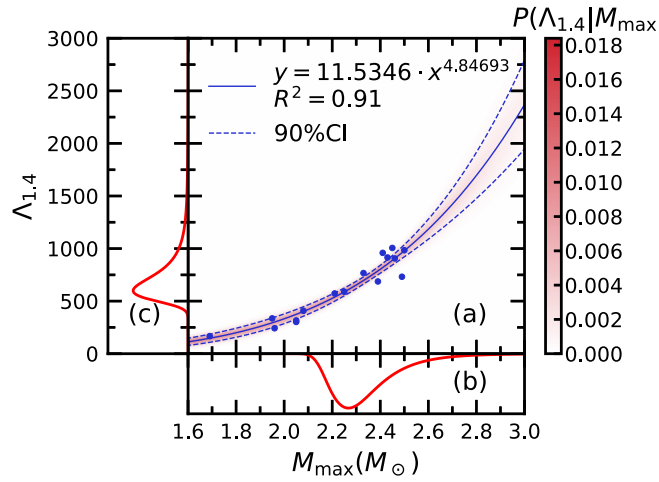


FIG. 1. (a) Tidal deformability of a 1.4-solar-mass NS, $\Lambda_{1.4}$, vs the NS mass limit $M_{\max}$, given by 16 different effective interactions (blue dots). The corresponding fitted line $\Lambda_{1.4} = 11.5346 M^{4.84693}_{\max}$ with a CoD of $R^2 = 0.91$ is plotted with a solid line. The PDF of $\Lambda_{1.4}$ for each $M_{\max}$, $P(\Lambda_{1.4}|M_{\max})$, is denoted by shades of red with a color bar, from which the 90% confidence interval is obtained and its boundaries are denoted by blue dashed lines. (b) The PDF of the NS mass limit $P(M_{\max}|\mathrm{EM})$ constrained by the NS mass observations taken from Ref. [14] is shown. (c) The yielded PDF of $\Lambda_{1.4}$ $P(\Lambda_{1.4}|\mathrm{EM})$ through the correlation between $\Lambda_{1.4}$ and $M_{\max}$ [see Eq. (2)] is shown.

yields the distribution $P(\Lambda_{1.4}|\mathrm{EM})$, which is shown in Fig. 1(c) as well as in Fig. 2 with the red dash-dotted line. The 90% confidence interval of this distribution gives $\Lambda_{1.4} = 675^{+543}_{-188}$.

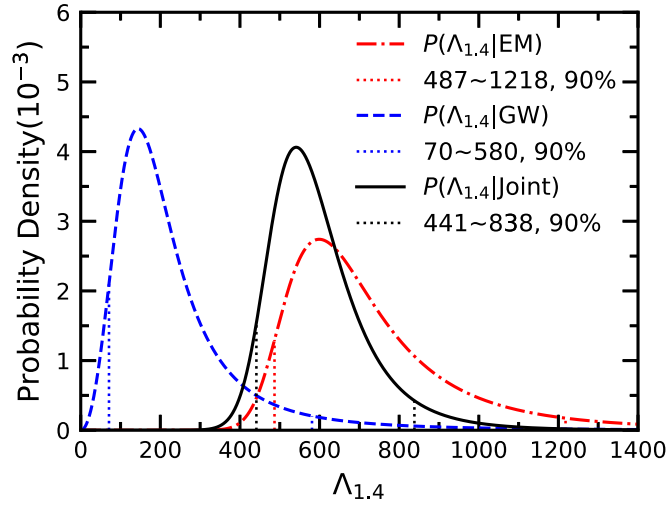


FIG. 2. The PDF of the tidal deformability of a 1.4-solar-mass NS, $\Lambda_{1.4}$, constrained by different messengers. $P(\Lambda_{1.4}|\mathrm{EM})$ constrained by supermassive NSs is denoted by a red dash-dotted line with the 90% confidence interval as $\Lambda_{1.4} = 675^{+543}_{-188}$. $P(\Lambda_{1.4}|\mathrm{GW})$ constrained by GW170817 is denoted by a blue dashed line which reproduces $\Lambda_{1.4} = 190^{+390}_{-120}$ [16]. The joint distribution $P(\Lambda_{1.4}|\mathrm{Joint})$ combining both messengers is denoted by a black solid line, with the 90% confidence interval as $\Lambda_{1.4} = 576^{+262}_{-135}$.

Besides the above yielded constraints on $\Lambda_{1.4}$ from the observation of NS masses, the direct constraint on $\Lambda_{1.4}$ from the NS merger event GW170817 is also known, which is $\Lambda_{1.4} = 190^{+290}_{-120}$ [16]. In order to get a PDF of $\Lambda_{1.4}$ that reproduces this constraint, we follow the procedure given in Ref. [52], which is also shown in Appendix B, and the corresponding result is shown in Fig. 2 with the blue dashed line. We notice that these two PDFs of $\Lambda_{1.4}$ are quite different. The EM-derived $M_{\rm max}$ pushed higher by the newly discovered NS PSR J0952 − 0607 prefers larger tidal deformabilities, resulting in a quite different PDF compared with the well-known one from GW170817. The larger tidal deformabilities preferred by NS mass limit compared to that given by GW170817 calls for more observations of NS mergers to constrain tidal deformabilities. As two independent constraints, we use the following joint distribution to combine the information from both messengers,

$$P(\Lambda_{1.4}|\text{Joint}) \propto P(\Lambda_{1.4}|\text{EM})P(\Lambda_{1.4}|\text{GW}), \tag{3}$$

which gives the black solid line in Fig. 2, with the 90% confidence interval being $\Lambda_{1.4} = 576^{+262}_{-135}$. Both bounds of this joint result are much higher than those constrained by GW170817, due to the influence of $P(\Lambda_{1.4}|\text{EM})$. Due to $P(\Lambda_{1.4}|\text{GW})$ from GW170817, the upper bound of the 90% confidence interval of the joint result is much lower than that of $P(\Lambda_{1.4}|\text{EM})$. Therefore, the joint distribution gives a comprehensive constraint on $\Lambda_{1.4}$ with information from both messengers being considered.

In order to convert the observation information of $\Lambda_{1.4}$ to the EoS, one needs to investigate correlations between the macroscopic properties of NSs and quantities in the EoS. Here, we find a surprisingly strong linear correlation between $\Lambda_{1.4}$ and the pressure $p(\rho)$ at each specific density in the range of $\rho_0$ to $5.6\rho_0$ with CoDs of $R^2 > 0.81$ (in the linear case $R^2 = r^2$, with $r$ being the Pearson's coefficient), as shown in Figs. 3(a) and 3(b). In particular, the correlation at density $\rho = 1.6\rho_0$ has the largest CoD of $R^2 = 0.992$. These good correlations allow us to constrain the EoS of NSs directly. Following the same procedure in Fig. 1, we can first obtain the PDF of pressure $p(\rho)$ at a given $\Lambda_{1.4}$, i.e., $P(p(\rho)|\Lambda_{1.4})$, using Eqs. (A1) and (A3) in Appendix A. Then combining the observation information $P(\Lambda_{1.4}|\text{Joint})$ [shown again in Fig. 3(c)] with the converter $P(p(\rho)|\Lambda_{1.4})$, the integration

$$P(p(\rho)|\text{Joint}) = \int \mathrm{d}\Lambda_{1.4} P(\Lambda_{1.4}|\text{Joint})P(p(\rho)|\Lambda_{1.4}) \tag{4}$$

yields the PDF of pressure $p(\rho)$ at each specific density $\rho$, i.e., $P(p(\rho)|\text{Joint})$ [shown in Figs. 3(d) and 3(e)], which gives exactly the NS EoS under multimessenger constraints.

By making $\rho$ vary continuously, we can obtain a constrained NS EoS after connecting the bounds of 90% (50%) confidence intervals of $P(p(\rho)|\text{Joint})$, shown as a light (dark) red band in Fig. 4. For comparison, the constrained EoS in Ref. [16], obtained through spectral parametrization taking into account the GW170817 mass configuration and the NS mass limit $M_{\rm max} > 1.97M_\odot$, is also shown with green bands. It can be seen that our constrained EoS has a remarkably lower uncertainty compared to that of Ref. [16]. At lower densities ($\rho \lesssim 1.6\rho_0$), our EoS prefers the upper bound of that in Ref. [16], but at higher densities ($\rho \gtrsim 4.0\rho_0$) our EoS prefers their lower bound. It means that our EoS shows a stiffer behavior at lower densities and a softer behavior at high densities.

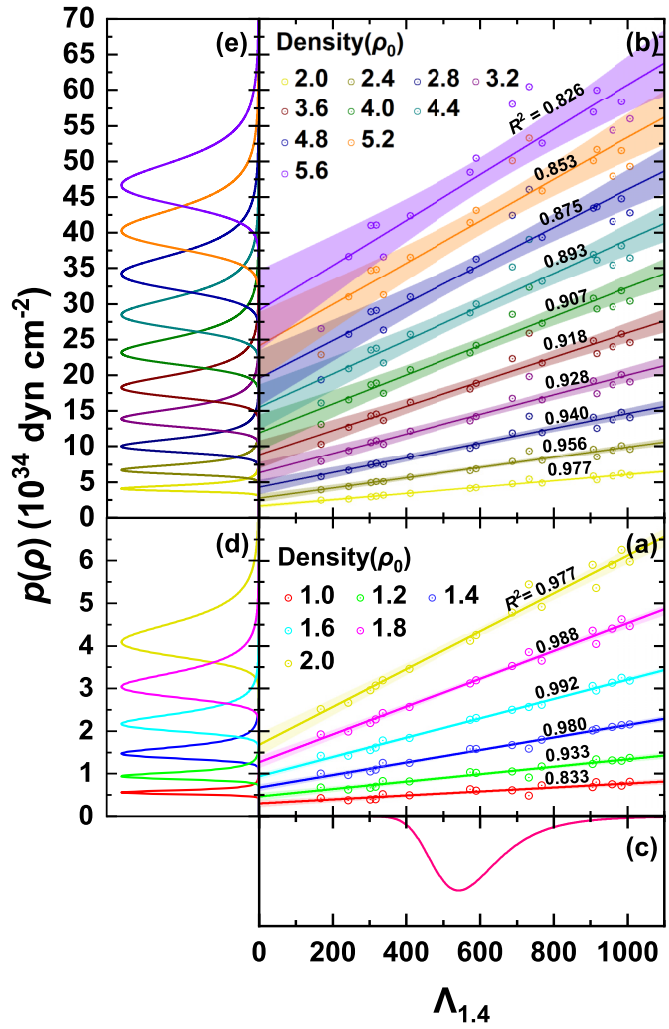


FIG. 3. Pressure at different densities $\rho = \rho_0$–$2.0\rho_0$ [panel (a)] and $\rho = 2.0\rho_0$–$5.6\rho_0$ [panel (b)] $p(\rho)$ vs tidal deformability of a 1.4-solar-mass NS, $\Lambda_{1.4}$, given by 16 different effective interactions (open circles). The linear fitted lines and the corresponding 90% confidence intervals are shown by solid lines and shaded areas, respectively, with the CoD $R^2$ on the top of each fitted line. The joint PDF of $\Lambda_{1.4}$, $P(\Lambda_{1.4}|\text{Joint})$, is shown in panel (c). The yielded PDF of pressure at each density $P(p(\rho)|\text{Joint})$ through the correlation between $p(\rho)$ and $\Lambda_{1.4}$ is shown in panel (d) for the density range $\rho = 1.0\rho_0$–$2.0\rho_0$ and in panel (e) for the density range $\rho = 2.0\rho_0$–$5.6\rho_0$.

The observation information from GW170817 and the NS mass limit are used to constrain the EoS in both our work and Ref. [16]. However, in Ref. [16], the NS mass constraints of $M_{\rm max} > 1.97M_\odot$ given by the $1\sigma$ lower mass bound of the previous heaviest NS PSR J0348 + 0432 discovered in 2013 [10] is considered, while in our work the state-of-the-art $M_{\rm max}$ distribution $P(M_{\rm max}|\text{EM})$ given in Ref. [14] including the novel heaviest NS PSR J0952 − 0607 is adopted. In order

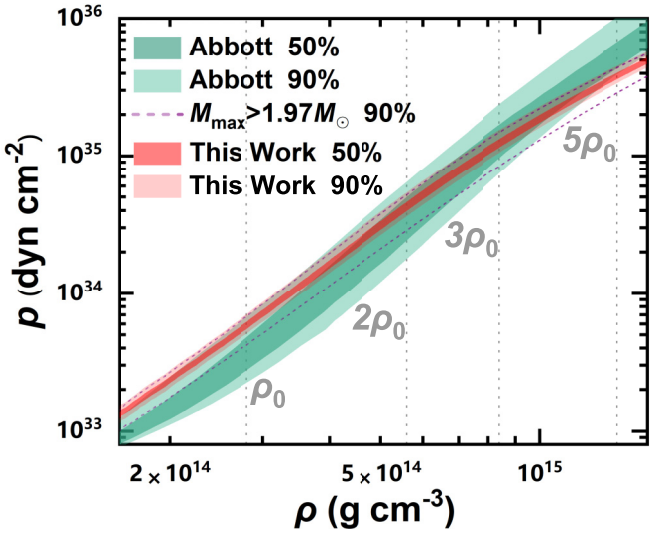


FIG. 4. The NS EoS $p(\rho)$ under different constraints. The light (dark) red shades denote the EoS constrained by $P(\Lambda_{1.4}|\text{Joint})$ containing information from both the GW event GW170817 [16] and the EM observations on supermassive NSs [14] with 90% (50%) confidence intervals. By replacing the NS mass limit to a distribution of $M_{\max} \in [1.97M_\odot, 3M_\odot]$, the constrained EoS with a 90% confidence interval is given by violet dashed lines. For comparison, the constrained EoS with a 90% (50%) confidence interval from Ref. [16] is also shown by the light (dark) green shades. Some representative densities are marked by gray dotted lines.

to exclude the effect of different observation information, we replace $P(M_{\max}|\text{EM})$ with the uniform distribution $M_{\max} \in [1.97M_\odot, 3M_\odot]$ whose lower bound is the same as that of Ref. [16]. Here, the upper bound is a conservative estimate of $M_{\max}$, which has a small impact on the result due to the extremely small $P(\Lambda_{1.4}|\text{GW})$ values at high $\Lambda_{1.4}$ values. The corresponding 90% confidence interval of the result after the replacement of the NS mass limit is shown with violet dashed lines in Fig. 4. It can be seen that the EoS with the same $M_{\max}$ constraint as Ref. [16] still shows a similar behavior as before, just with larger uncertainties. It means that although our EoS is obtained under the pure $npe\mu$ core hypothesis, it still prefers stiffer NS EoSs at lower densities and softer ones at higher densities with the same information considered, compared with that in Ref. [16], where no hypothesis on NS components is made. It tells us the nucleonic interaction is able to give softer behavior at high densities without the inclusion of extra degrees of freedom, and this phenomenon has the potential to be used as an indicator for the components of the NS core.

Furthermore, our constrained EoS has a much smaller uncertainty than that of Ref. [16] even with the same observation information considered, due to the innovative constraining method making use of the newly discovered $p$-$\Lambda_{1.4}$ correlation. It shows that the $p$-$\Lambda_{1.4}$ correlation is verified not only as a quick converter but also as an efficient constraint on the EoS. With the inclusion of more advanced observation information, the uncertainty of the EoS is further reduced from violet dashed lines to the light red region, which shows the importance of new observations, and the new observation information could be efficiently transferred into the EoS through our constraining method. Therefore, our method could serve as a useful converter between future advances in observation of NSs and the EoS.

In summary, we proposed a novel method to constrain the NS EoS through the linear correlation between the pressure of the NS at each density and the tidal deformability of a 1.4-solar-mass NS based on various density functionals including both relativistic and nonrelativistic ones. Apart from the tidal deformability constraints from GW170817, the observation information of the NS mass limit, especially the novel NS mass limit given by NS PSR J0952 − 0607, is also transferred to the constraints on tidal deformability through the correlation between them. With the efficient constraining method and the most advanced observation information of NSs, our yielded EoS has a very small uncertainty, which shows our method could serve as a useful converter between observations of NSs and the EoS. The newly constrained EoS shows a stiffer behavior at lower densities and a softer behavior at higher densities compared to that of Ref. [16] without the inclusion of extra degrees of freedom, which shows its potential to be used as an indicator for the components of the NS core.

With this adaptable new approach, future development of observation of NSs can be directly converted to the constraints on the NS EoS, which will further deepen our understanding of the EoS as well as the components of NSs.

This work is supported by the National Key Research and Development (R&D) Program under Grant No. 2021YFA1601500 and the National Natural Science Foundation of China under Grant No. 12075104.

*Appendix A: Conditional probability distribution function.* The correlation between two data sets $(x_i, y_i)$ is modeled by the function $\hat{y} = f(x)$ using the least-square method. For a given $x$, the $y$ values follow the conditional PDF $P(y|x)$, which is obtained using a $t$ distribution with degrees of freedom of $n-2$ [53]:

$$P(y|x) = \frac{\Gamma\left(\frac{n-1}{2}\right)}{\sqrt{(n-2)\pi}\,\Gamma\left(\frac{n-2}{2}\right)}\left[1 + \frac{(y-\hat{y})^2}{(n-2)\sigma^2 \text{Var}}\right], \quad \text{(A1)}$$

where $\Gamma(x)$ is the Gamma function; $\sigma^2$ is the variance of the population error, which is usually unknown, and it is usually unbiased estimated by the mean-squared error $S^2 = \sum_i (y_i - \hat{y}_i)^2/(n-2)$, with $\hat{y}_i = f(x_i)$; and Var is the variance of the fitting model given by the well-known $\Delta$ method [54]. For a power-law fitting, the model variance is given as

$$\text{Var}[ax^b] = \frac{x^{2b}\left[\sum x_i^{2b} \ln^2 x_i - 2\ln x \sum x_i^{2b} \ln x_i + \ln^2 x \sum x_i^{2b}\right]}{\left(\sum x_i^{2b} \ln^2 x_i\right)\sum x_i^{2b} - \left(\sum x_i^{2b} \ln x_i\right)^2}, \quad \text{(A2)}$$

and for a linear fitting, the model variance is given as

$$\text{Var}[ax+b] = \frac{nx^2 - 2x\sum x_i + \sum x_i^2}{n\sum x_i^2 - \left(\sum x_i\right)^2}, \quad \text{(A3)}$$

where $n$ is the sample size, and $a$ and $b$ are model parameters.

Following the above formulas, for $\{M^i_{\rm max}, \Lambda^i_{1.4}\}$, after a power-law fitting, the conditional PDF of the tidal deformability $\Lambda_{1.4}$ at a given $M_{\rm max}$, $P(\Lambda_{1.4}|M_{\rm max})$, is obtained; and similarly for $\{\Lambda^i_{1.4}, p^i(\rho)\}$, after a linear fitting, the conditional PDF of pressure $p$ for a specific density $\rho$ at a given tidal deformability $\Lambda_{1.4}$, $P(p(\rho)|\Lambda_{1.4})$, is also obtained.

*Appendix B: Probability distribution function of* $\Lambda_{1.4}$ *from GW170817.* In Ref. [16], the GW170817 event gives the constraints on tidal deformability of a 1.4-solar-mass neutron star, $\Lambda_{1.4} = 190^{+390}_{-120}$. In order to get the PDF of $\Lambda_{1.4}$ which reproduces this constraints, we use the so-called generalized $\beta$ distribution of the second kind (GB2) like Ref. [52] does,

$$\mathrm{GB2}(x; p, q, \alpha, \beta) = \frac{\alpha(1 + (x/\beta)^\alpha)^{-p-q}(x/\beta)^{p\alpha-1}}{\beta B(p, q)}, \quad \text{(B1)}$$

with $B(p, q)$ being the Beta function. Here the parameters are adjusted to be $\alpha = 3$, $\beta = 170.97$, $p = 1.02$, and $q = 0.82$ in order to reproduce $\Lambda_{1.4} = 190^{+390}_{-120}(90\%)$. The resulting distribution is denoted as $P(\Lambda_{1.4}|\mathrm{GW}) = \mathrm{GB2}(\Lambda_{1.4}; p, q, \alpha, \beta)$.


[1] A. Sorensen, K. Agarwal, K. W. Brown, Z. Chajęcki, P. Danielewicz, C. Drischler, S. Gandolfi, J. W. Holt, M. Kaminski, C.-M. Ko *et al.*, Prog. Part. Nucl. Phys. **134**, 104080 (2024).
[2] F. Özel and P. Freire, Annu. Rev. Astron. Astrophys. **54**, 401 (2016).
[3] J. M. Lattimer and M. Prakash, Science **304**, 536 (2004).
[4] R. C. Tolman, Phys. Rev. **55**, 364 (1939).
[5] J. R. Oppenheimer and G. M. Volkoff, Phys. Rev. **55**, 374 (1939).
[6] T. Hinderer, Astrophys. J. **677**, 1216 (2008).
[7] C. G. Bassa, Z. Pleunis, J. W. T. Hessels, E. C. Ferrara, R. P. Breton, N. V. Gusinskaia, V. I. Kondratiev, S. Sanidas, L. Nieder, C. J. Clark *et al.*, Astrophys. J. Lett. **846**, L20 (2017).
[8] E. Fonseca, H. T. Cromartie, T. T. Pennucci, P. S. Ray, A. Y. Kirichenko, S. M. Ransom, P. B. Demorest, I. H. Stairs, Z. Arzoumanian, L. Guillemot *et al.*, Astrophys. J. Lett. **915**, L12 (2021).
[9] H. T. Cromartie, E. Fonseca, S. M. Ransom, P. B. Demorest, Z. Arzoumanian, H. Blumer, P. R. Brook, M. E. DeCesar, T. Dolch, J. A. Ellis *et al.*, Nat. Astron. **4**, 72 (2020).
[10] J. Antoniadis, P. C. C. Freire, N. Wex, T. M. Tauris, R. S. Lynch, M. H. Van Kerkwijk, M. Kramer, C. Bassa, V. S. Dhillon, T. Driebe *et al.*, Science **340**, 1233232 (2013).
[11] R. W. Romani, D. Kandel, A. V. Filippenko, T. G. Brink, and W.-K. Zheng, Astrophys. J. Lett. **908**, L46 (2021).
[12] M. Linares, T. Shahbaz, and J. Casares, Astrophys. J. **859**, 54 (2018).
[13] D. Kandel and R. W. Romani, Astrophys. J. **892**, 101 (2020).
[14] R. W. Romani, D. Kandel, A. V. Filippenko, T. G. Brink, and W.-K. Zheng, Astrophys. J. Lett. **934**, L17 (2022).
[15] B. P. Abbott *et al.*, Phys. Rev. Lett. **119**, 161101 (2017).
[16] B. P. Abbott *et al.*, Phys. Rev. Lett. **121**, 161101 (2018).
[17] B.-A. Li, B.-J. Cai, W.-J. Xie, and N.-B. Zhang, Universe **7**, 182 (2021).
[18] C. Y. Tsang, M. B. Tsang, P. Danielewicz, W. G. Lynch, and F. J. Fattoyev, Phys. Rev. C **102**, 045808 (2020).
[19] L. Lindblom and N. M. Indik, Phys. Rev. D **86**, 084003 (2012).
[20] L. Lindblom, Phys. Rev. D **82**, 103011 (2010).
[21] L. Lindblom and N. M. Indik, Phys. Rev. D **93**, 129903(E) (2016).
[22] K. Hebeler, J. M. Lattimer, C. J. Pethick, and A. Schwenk, Astrophys. J. **773**, 11 (2013).
[23] A. Kurkela, E. S. Fraga, J. Schaffner-Bielich, and A. Vuorinen, Astrophys. J. **789**, 127 (2014).
[24] E. Annala, T. Gorda, A. Kurkela, and A. Vuorinen, Phys. Rev. Lett. **120**, 172703 (2018).
[25] E. Annala, T. Gorda, E. Katerini, A. Kurkela, J. Nättilä, V. Paschalidis, and A. Vuorinen, Phys. Rev. X **12**, 011058 (2022).
[26] E. Annala, T. Gorda, A. Kurkela, J. Nättilä, and A. Vuorinen, Nat. Phys. **16**, 907 (2020).
[27] Y. Lim and J. W. Holt, Phys. Rev. Lett. **121**, 062701 (2018).
[28] T. Malik, N. Alam, M. Fortin, C. Providência, B. K. Agrawal, T. K. Jha, B. Kumar, and S. K. Patra, Phys. Rev. C **98**, 035804 (2018).
[29] J. Piekarewicz and F. J. Fattoyev, Phys. Rev. C **99**, 045802 (2019).
[30] C. Y. Tsang, M. B. Tsang, P. Danielewicz, F. J. Fattoyev, and W. G. Lynch, Phys. Lett. B **796**, 1 (2019).
[31] R. Nandi, P. Char, and S. Pal, Phys. Rev. C **99**, 052802(R) (2019).
[32] M. Fortin, C. Providência, A. R. Raduta, F. Gulminelli, J. L. Zdunik, P. Haensel, and M. Bejger, Phys. Rev. C **94**, 035804 (2016).
[33] M. B. Tsang, W. G. Lynch, P. Danielewicz, and C. Y. Tsang, Phys. Lett. B **795**, 533 (2019).
[34] Y.-X. Zhang, M. Liu, C.-J. Xia, Z.-X. Li, and S. K. Biswal, Phys. Rev. C **101**, 034303 (2020).
[35] T. Malik, B. K. Agrawal, J. N. De, S. K. Samaddar, C. Providência, C. Mondal, and T. K. Jha, Phys. Rev. C **99**, 052801(R) (2019).
[36] G. Baym, C. Pethick, and P. Sutherland, Astrophys. J. **170**, 299 (1971).
[37] G. Baym, H. A. Bethe, and C. J. Pethick, Nucl. Phys. A **175**, 225 (1971).
[38] L.-W. Chen, C. M. Ko, B.-A. Li, and J. Xu, Phys. Rev. C **82**, 024321 (2010).
[39] N. Van Giai and H. Sagawa, Phys. Lett. B **106**, 379 (1981).
[40] M. Beiner, H. Flocard, N. Van Giai, and P. Quentin, Nucl. Phys. A **238**, 29 (1975).
[41] H. Köhler, Nucl. Phys. A **258**, 301 (1976).
[42] H. Krivine, J. Treiner, and O. Bohigas, Nucl. Phys. A **336**, 155 (1980).
[43] E. Chabanat, Ph.D. thesis, Lyon-1 Université, 1995.
[44] B. K. Agrawal, S. Shlomo, and V. K. Au, Phys. Rev. C **72**, 014310 (2005).
[45] X. Roca-Maza, G. Colò, and H. Sagawa, Phys. Rev. C **86**, 031306(R) (2012).
[46] G. A. Lalazissis, T. Nikšić, D. Vretenar, and P. Ring, Phys. Rev. C **71**, 024312 (2005).

[47] S. Typel and H. H. Wolter, Nucl. Phys. A **656**, 331 (1999).
[48] W.-H. Long, H. Sagawa, N. V. Giai, and J. Meng, Phys. Rev. C **76**, 034314 (2007).
[49] W.-H. Long, J. Meng, N. Van Giai, and S.-G. Zhou, Phys. Rev. C **69**, 034319 (2004).
[50] W.-H. Long, N. Van Giai, and J. Meng, Phys. Lett. B **640**, 150 (2006).
[51] W.-H. Long, H. Sagawa, J. Meng, and N. Van Giai, Europhys. Lett. **82**, 12001 (2008).
[52] B. Kumar and P. Landry, Phys. Rev. D **99**, 123026 (2019).
[53] J. M. Wooldridge, *Introductory Econometrics: A Modern Approach* (Cengage Learning, Boston, 2015).
[54] J. R. Donaldson and R. B. Schnabel, Technometrics **29**, 67 (1987).